WELDING RESEARCH

SUPPLEMENT TO THE *WELDING JOURNAL*, SEPTEMBER 2014
Sponsored by the American Welding Society and the Welding Research Council

Active Metal Transfer Control by Utilizing Enhanced Droplet Oscillation Part II: Modeling and Analysis

The model suggests that the exciting phase delay and exciting peak duration can be fixed as long as the droplet size is controlled to be relatively small

BY J. XIAO, G. J. ZHANG, W. J. ZHANG, AND Y. M. ZHANG

ABSTRACT

Enhanced active metal transfer control is experimentally studied in the first part of this investigation. Differing from the original active control, the enhanced active metal transfer control uses a modified current waveform, which increases the amplitude of the excited droplet oscillation and the needed detaching current is thus much more reduced. The experimental study reveals that strongest droplet oscillation and maximum enhancement on the droplet detachment require optimal selections of three waveform parameters: the exciting peak duration and exciting/detaching phase delay. In this study, a numerical model on the dynamic droplet oscillation and detachment is developed based on the mass-spring system. The spring constant and damping coefficient in the model are experimentally calibrated. Analysis on the effects of the key waveform parameters on the droplet oscillation/detachment gives a comprehensive understanding on the mechanism of the droplet excitation and detachment. Given other waveform parameters, the optimal value of the three key parameters can be calculated from the model. The accuracy of the model is verified by comparing the modeling results with the corresponding experimental ones. The modeling results suggest that the exciting phase delay and exciting peak duration can be fixed as long as the droplet size is controlled to be relatively small as desired by the drop spray transfer. In addition, an analytical model has been established through approximations, and its adequate accuracy in predicting the optimal detaching phase delay has also been verified.

KEYWORDS

• Enhanced Active Control • Metal Transfer • Droplet Oscillation
• Theoretical Model • Mass-Spring System

Introduction

As has been reviewed in the first part of this paper (Ref. 1) and previous studies, the detaching peak current in conventional pulsed gas metal arc welding (GMAW-P) needs to be higher than the spray transition current to produce desired one drop per pulse (ODPP) transfer. Further, the ODPP transfer in conventional GMAW-P lacks controllability and robustness (Refs. 2–5). The original version of the active metal transfer control method is thus proposed, in which the liquid droplet is effectively excited into oscillation by reducing the welding current from a peak level, referred to as the exciting peak, to the base. By applying another peak current referred to as the detaching peak at the moment when the droplet is moving toward the weld pool, the electromagnetic force and the downward momentum of the oscillating droplet are effectively matched in phase and the droplet can be detached by their combined action. As a result, the needed detaching current is reduced, and unexpected droplet detachment or mass accumulation can be avoided such that the metal transfer robustness is improved (Refs. 6, 7).

As an evolution to the original active control process, the enhanced active droplet oscillation is proposed in Ref. 8 by using the current waveform shown in Fig. 1 and denoted as Wave1. The droplet growing and exciting pulses are now divided by a base period, while they are coupled together in the original active metal transfer control. It is this modification that significantly increases the amplitude of the excited droplet oscillation (Ref. 8). Active metal transfer control, which utilizes such enhanced oscillation, referred to as the enhanced active metal transfer control, has been experimentally studied in the first part of this investigation (Ref. 1) by using Wave2, which inherits from Wave1 by inserting a relatively low detaching pulse with a phase delay to the exciting pulse, as shown in Fig. 2. The enhanced droplet oscillation enables the needed

J. XIAO is with the State Key Laboratory of Advanced Welding and Joining, Harbin Institute of Technology, China, and the Institute for Sustainable Manufacturing, University of Kentucky, Lexington, Ky. G. J. ZHANG is with the State Key Laboratory of Advanced Welding and Joining, Harbin Institute of Technology, China. W. J. ZHANG and Y. M. ZHANG (yuming.zhang@uky.edu) *are with the Institute for Sustainable Manufacturing and Department of Electrical and Computer Engineering, University of Kentucky, Lexington, Ky.*

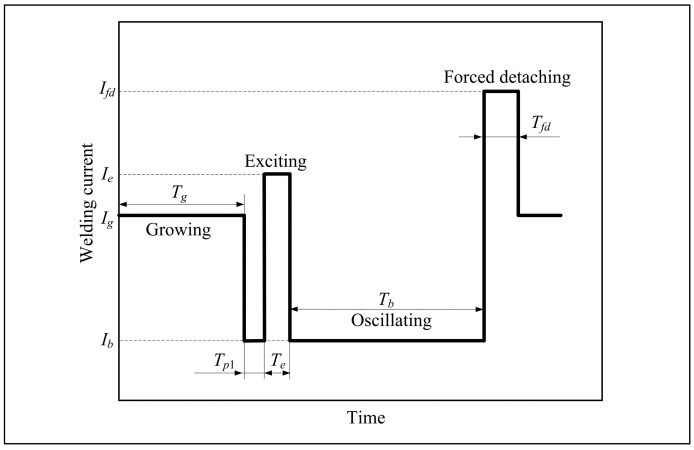

Fig. 1 — Current waveform for enhanced droplet oscillation.

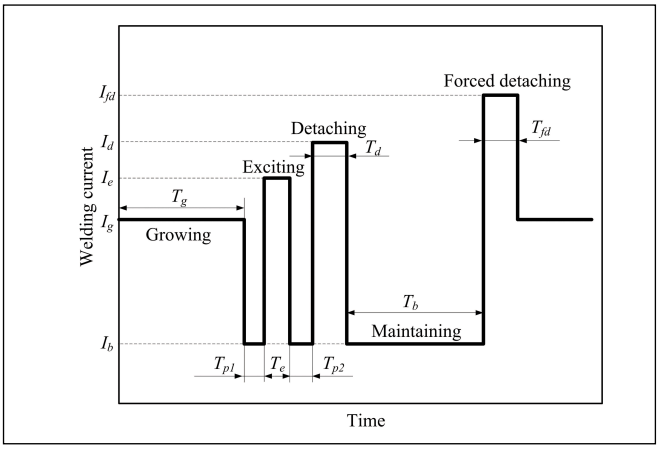

Fig. 2 — Current waveform for enhanced active metal transfer control.

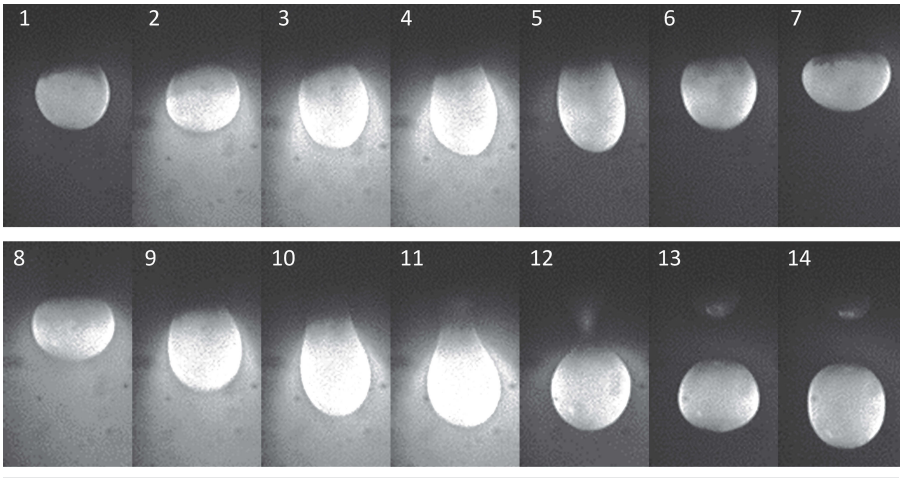

Fig 3 — Typical metal transfer of enhanced active control, 1 ms per frame. ER70S-6/0.8-mm wire, 15L/min argon gas flow, 6-mm arc length, 6-mm wire extension, bead-on-plate welding.

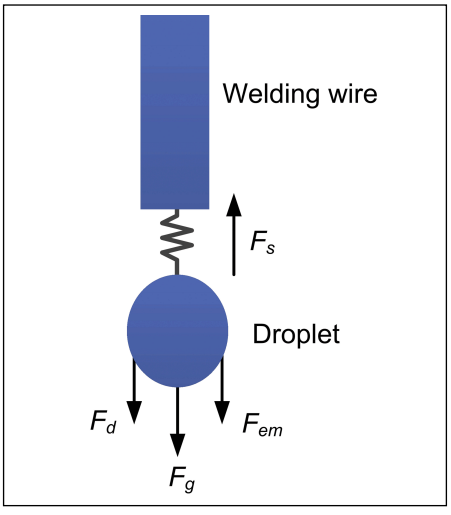

Fig. 4 — Illustration of mass-spring model of droplet oscillation.

detaching current to be further reduced. The lower limit of the detaching current is determined to be not only much lower than the spray transition current, but also significantly lower than that of the original active metal transfer control. The experimental study also indicates that the enhanced active metal transfer control process is sufficiently robust (Ref. 1).

Figure 3 demonstrates a typical droplet excitation and detachment in the enhanced active metal transfer control where Wave2 is used: I_g = 80 A, T_g = 20 ms, I_b = 30 A, T_{p1} = 2 ms, I_e = 120 A, T_e = 3 ms, T_{p2} = 3.2 ms, I_d = 125 A, and T_d = 4 ms, T_b = 20 ms, I_{fd} = 175 A, T_{fd} = 5 ms. It can be seen that the droplet is first elongated by the exciting pulse (Frames 2–4) and goes into oscillation in the base period called detaching phase delay (Frames 5–7), and then the droplet is accelerated and detached by the detaching pulse of only 125 A/4 ms (Frames 8–13).

To better depict the excited droplet oscillation, the following concepts defined in the experimental study are repeated here. 1) The moment at which the excited droplet reaches its maximum elongation is referred to as the elongation peak moment. 2) The moment at which the droplet changes its moving direction from upward (toward the wire) into downward (away from the wire) during the preoscillation or the main oscillation is referred to as the oscillation reversing moment. As can be seen from Fig. 2, the following current waveform parameters need to be properly selected to first maximize the droplet oscillation amplitude and then maximize the consequent enhancement on the droplet detachment in the enhanced active metal transfer control.

1. *Exciting phase delay* T_{p1}, i.e., the base duration between the growing and exciting pulse. As has been verified in Ref. 8, the droplet may be excited to a preoscillation during T_{p1} as long as the growing current is high enough to preelongate the droplet. If the exciting pulse is synchronized with the downward momentum during the preoscillation, the main oscillation after the exciting pulse can be further enhanced. If the growing current is sufficiently low, for example, 80 A used in the experimental study, the selection of T_{p1} will not affect the main droplet oscillation significantly. In this sense, this parameter was not discussed in the experimental study, but it will be analyzed in this theoretical study.

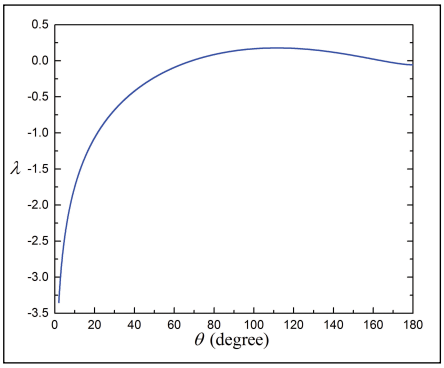

Fig. 5 — Variation of λ as the function of half angle.

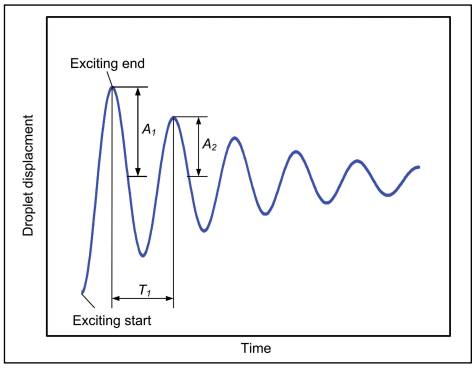

Fig. 6 — Illustration of damping coefficient measurement.

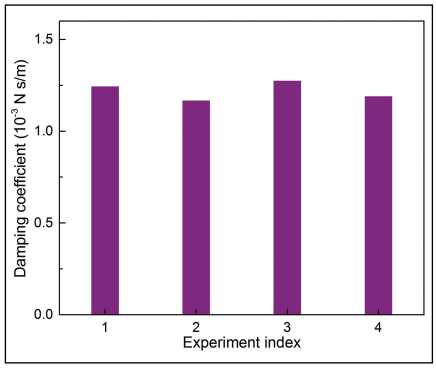

Fig. 7 — Damping coefficient measured from experiments 1–4.

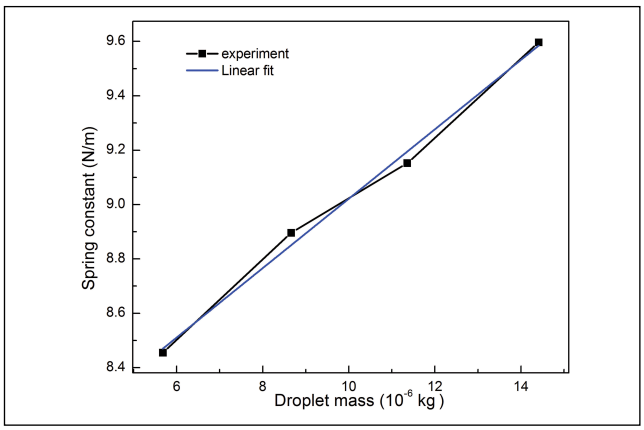

Fig. 8 — Correlation between spring constant and droplet mass.

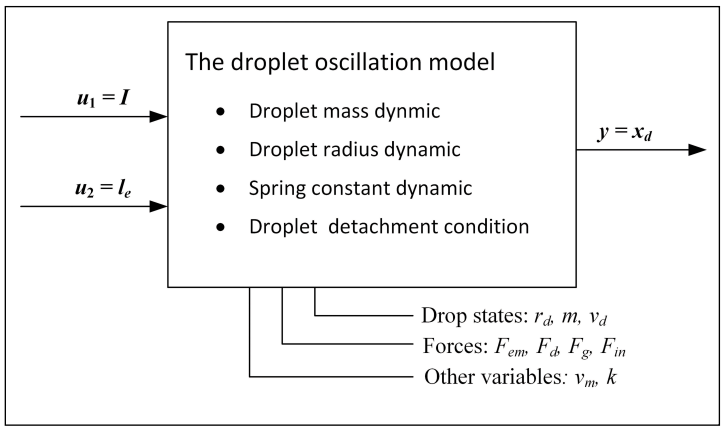

Fig. 9 — Structure of the Simulink program.

2. *Exciting peak duration* T_e. Experimental study on the enhanced droplet oscillation demonstrates that there is an optimal exciting peak duration for achieving strongest droplet oscillation when the exciting peak current is the same (Ref. 8). Exciting peak duration greater than the optimal value is not recommended because it not only reduces the oscillation amplitude but also increases the heat input.

3. *Detaching phase delay* T_{p2}, i.e., the base duration between the exciting and detaching pulse. This is the most important parameter for the enhanced active metal transfer control, because it determines if the droplet oscillation can be effectively utilized. In particular, if the detaching pulse starts exactly at the oscillation reversing moment, the resultant detaching phase delay is called feature detaching phase delay, denoted as T^*_{p2}. It has been verified that the feature detaching phase delay is the optimal selection for full utilization of the droplet oscillation.

Experimental determination of the optimal value of these parameters is time-consuming and costly such that it will not be preferred in manufacturing. Hence, a theoretical model on the dynamic droplet oscillation/detachment is needed. Such a model would be highly appreciated since it enables to predict the critical waveform parameters in a cost-effective way. Further, the model will give a deeper scientific understanding on the mechanism of the droplet oscillation and detachment. Together with the experimental work conducted in the first part of this investigation, the theoretical modeling and analysis complete a full study on the enhanced active metal transfer control.

Objective and Method

The task now is to establish a theoretical model on the dynamic droplet oscillation and detachment under the current waveform shown in Fig. 2. The model will be used to predict the critical waveform parameters in the enhanced active metal transfer control when other waveform parameters are given:

1. Optimal exciting phase delay T^*_{p1}, which is the time interval between the reversing moment of the preoscillation and the end moment of the growing pulse.

2. Optimal exciting peak duration T^*_e, under which the end moment of the exciting pulse is exactly the elongation peak moment.

3. Optimal detaching phase delay T^*_{p2}, which is the time interval between the reversing moment of the excited droplet oscillation and the end moment of the exciting pulse.

Mass-spring system has been widely used to model the pendant droplet oscillation in GMAW under different current conditions (Refs. 9–12). It is also used in this study to model the enhanced droplet oscillation and detachment under the waveform as Fig. 2 shows. The modeling is facilitated by the following assumptions: 1) the droplet shape is symmetric; 2) the droplet motion in the wire redial direc-

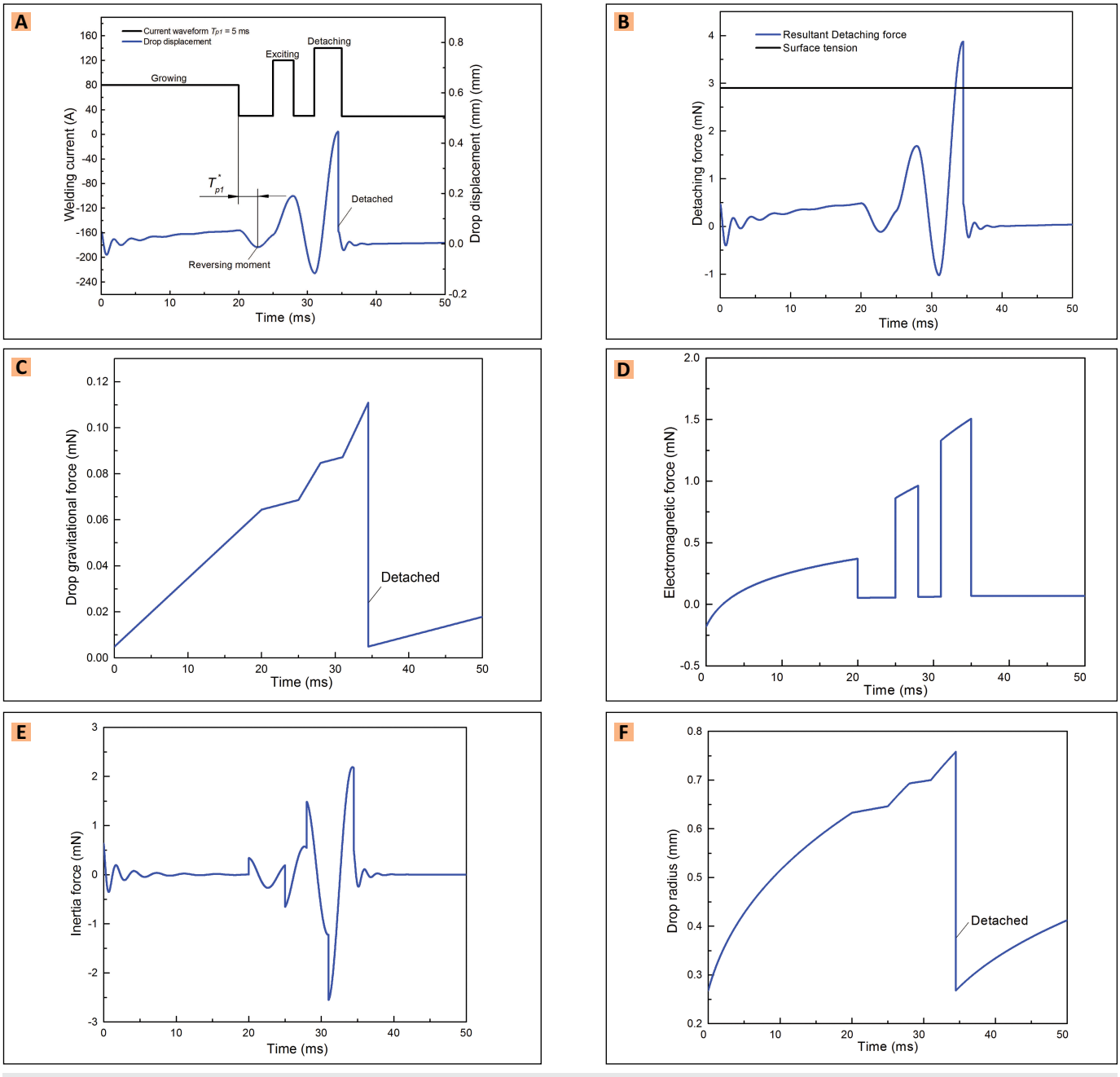

Fig. 10 — Modeling results of the dynamic droplet oscillation and detachment. A — Droplet displacement; B — resultant detaching force; C — droplet gravitational force; D — electromagnetic force; E — inertia force; F — droplet radius.

tion is negligible; and 3) the physical property of the liquid metal is constant.

Figure 4 shows the mass-spring model for pendant droplet oscillation in GMAW. The surface tension acts as the spring force F_s. Since the droplet volume increases continuously until its detachment, the oscillation system varies with time and follows the governing equations:

$$m\ddot{x} + b\dot{x} + kx = F(t) \quad (1)$$

$$F(t) = F_{em} + F_d + F_g \quad (2)$$

where x represents the droplet mass center displacement to the wire tip in the wire axial direction; m, b, and k are the mass, damping coefficient, and spring constant, respectively. F is the axial force exerted on the droplet, including the electromagnetic force F_{em}, the plasma drag force F_d, and the droplet gravitational force F_g.

The droplet mass is proportional to the wire melting speed (Ref. 13):

$$m(t) = \int \rho \cdot v_m(t)dt \quad (3)$$

where ρ represents the mass density of the wire, v_m the wire melting speed, which is the function of the welding current and wire extension (Ref. 13)

$$v_m = C_1 I(t) + C_2 \rho_r l_e(t) I^2(t) \quad (4)$$

where I represents the welding current, l_e the wire extension, ρ_r the wire resis-

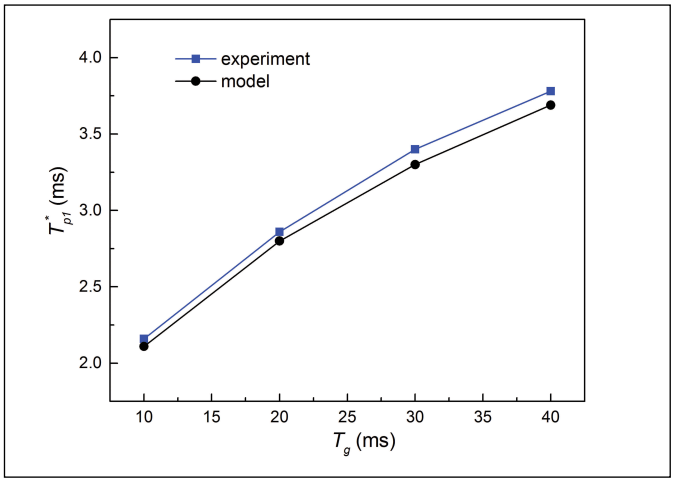

Fig. 11 — T^*_{p1} under different T_g.

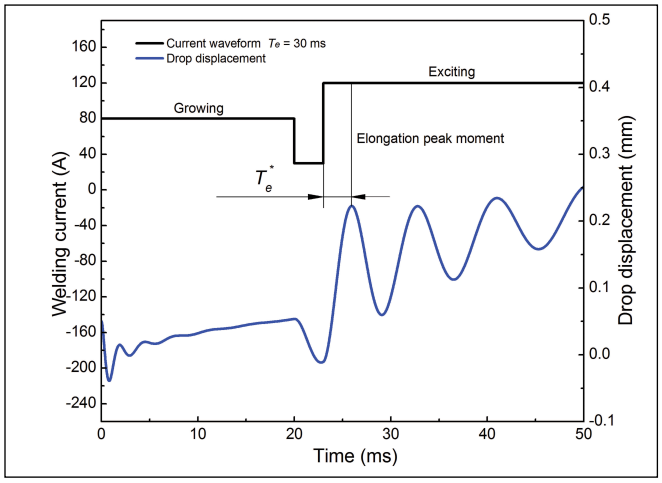

Fig. 12 — Droplet dynamic response to exciting pulse.

tivity, plus C_1 and C_2 the melting constants. The first term in the right side of Equation 4 represents the arc anode heat while the second term represents the wire resistive heat. Hence, given the current waveform, the droplet mass can be obtained.

The droplet gravitational force F_g is given by

$$F_g(t) = m(t)g = \tfrac{4}{3}\,\pi r_d(t)^3 \rho' g \qquad (5)$$

where r_d is the droplet radius, and ρ' represents the density of liquid droplet.

The electromagnetic force F_{em} is given by (Ref. 14)

$$F_{em}(t) = \frac{\mu_0 I^2(t)}{4\pi}\left[ln\frac{r_d(t)}{r_w} + \lambda\right] \qquad (6)$$

$$\lambda = 1n(sin\theta) - \frac{1}{4} - \frac{1}{1-cos\theta} + \frac{2}{(1-cos\theta)^2} ln\frac{2}{1+cos\theta} \qquad (7)$$

where μ_0 is the magnetic permittivity, I is the welding current, r_w the wire radius, and θ is the half angle subtended by the arc root at the center of the droplet. Figure 5's graphical illustration of Equation 7 shows that λ does not change significantly when the half angle ranges from 90 to 150 deg, so that the selection of the half angle would not significantly influence the modeling results, and the half angle θ is fixed at 120 deg in this study. References 15 and 16 also use constant half angle to calculate the electromagnetic force for the same reason.

The plasma drag force is given by (Ref. 15)

$$F_d = \frac{1}{2} C_d A_p \rho_p v_p^2 \qquad (8)$$

$$A_p = \pi\left(r_d^2 - r_w^2\right) \qquad (9)$$

where C_d is the aerodynamic drag coefficient, A_p is the area of the drop seen from above, and ρ_p and v_p are the density and velocity of the arc plasma. Since the plasma velocity in GMAW is not available, the plasma velocity was assumed to be 100 m/s, which is the same as that in GTAW, and the value of C_d was calculated to be 0.44 (Ref. 15). For a less-developed plasma jet, 10 m/s plasma velocity was used, and the value of C_d was also calculated to be 0.44. The calculation in Ref. 15 shows that the equilibrium droplet size of a steel electrode with plasma velocity of 10 m/s and 100 m/s are almost the same. Thus, in this study, 100 m/s plasma velocity is used, and the drag coefficient is thus 0.44.

According to the dynamic force balance theory on the metal transfer (Ref. 9), the droplet will be detached when the following criteria are satisfied:

$$F_{em} + F_d + F_g + F_{in} > F_\sigma \qquad (10)$$

where F_{in} is the inertia force generated by the oscillation, $F_{in} = -ma$, and a represents the droplet acceleration. F_σ is the surface tension, given by

$$F_\sigma = 2\pi r_w \gamma \qquad (11)$$

where γ is the surface tension coefficient.

Calibration of Model Coefficients

To solve Equation 1, the spring constant k and damping coefficient b need to be determined first. It is the major difficulty in our modeling effort because the spring constant and damping coefficient may change with the droplet mass even if the wire (material, diameter) and shielding gas are given. The theoretical models on the spring constant and damping coefficient are briefly reviewed here. The spring force and spring constant in the axial direction are expressed using the potential energy generated by the surface tension and surface area of a droplet in Ref. 9

$$dU = \gamma dS = F_s dx,\ k = dF_s/dx$$

where U is the potential energy, F_s the spring force, γ the surface tension coefficient and S the drop surface area. Given the droplet mass/volume, the spring constant can be calculated. Unfortunately, the accuracy of this model is not satisfactory (minimum 11% error and 38% maximum in the droplet oscillation frequency), and it is thus not used in this paper. However, it indicates that the droplet spring constant is related to the droplet mass/volume. Reference 9 also gives

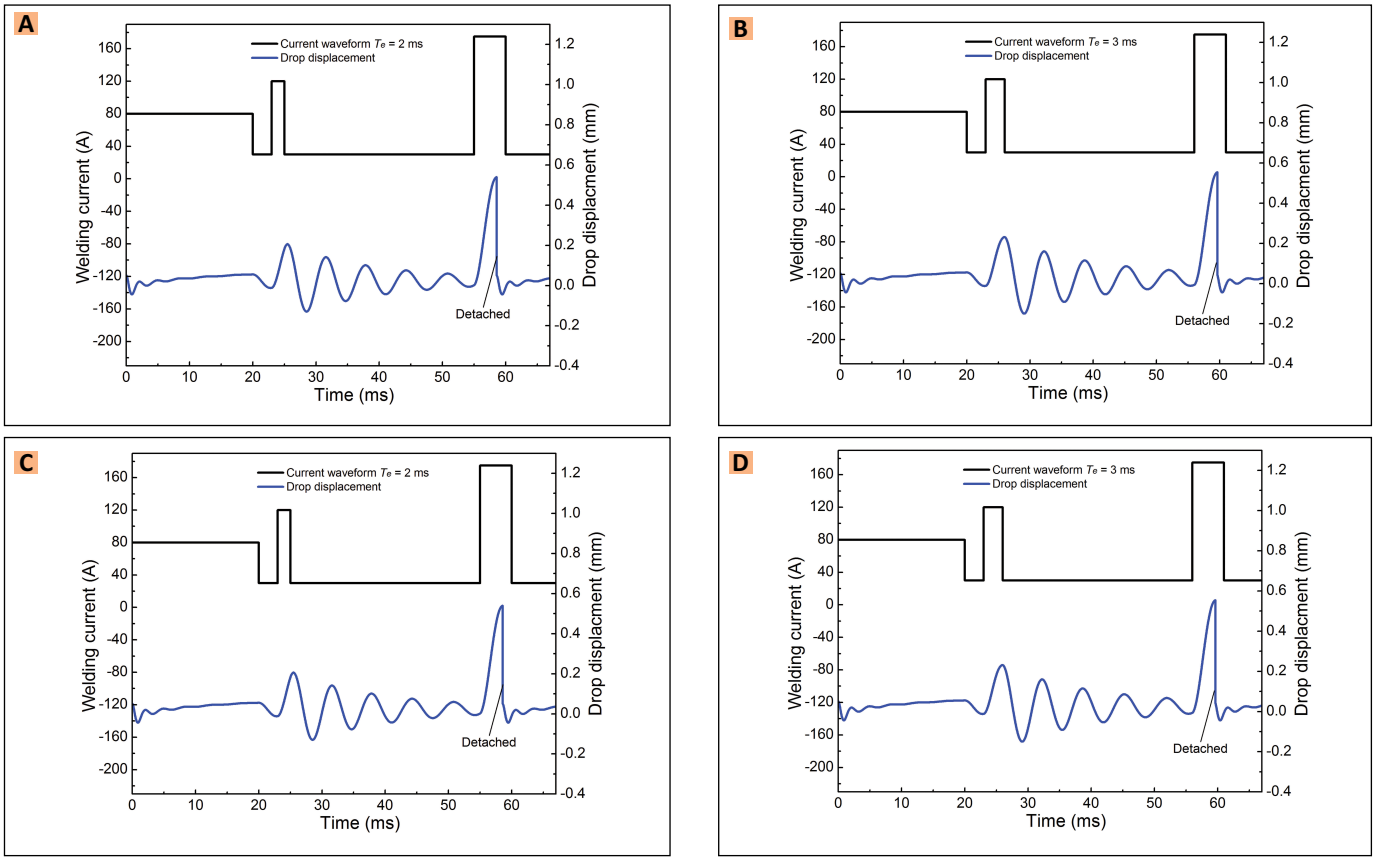

Fig. 13 — Droplet oscillation under different T_e *. A —* T_e *= 2 ms; B —* T_e *= 3 ms; C —* T_e *= 4 ms; D —* T_e *= 5 ms.*

the damping coefficient as

$$b = 3\mu V/x^2$$

where μ is the viscosity coefficient, V is the droplet volume, and x the droplet displacement. Using this model, the damping coefficient is calculated to be only at the order of $10^{-5} - 10^{-4}$ N/m, which does not match the real damping observed in the experiments. Hence, this model for calculating the damping coefficient is also not used in this study. Thereby, the two key variables need to be experimentally calibrated.

Calibration Method

The calibration proceeds with the assumption that the droplet mass during the first free oscillation period after the exciting pulse is constant, since the wire melting rate at the base current is sufficiently low and the concerned period, the first oscillation cycle after the exciting pulse, is only a few milliseconds. As a result, the droplet mass during the first oscillation cycle can be considered equal to the droplet mass m_0 measured at the end moment of the exciting pulse. In this case, the droplet mass m, the damping factor b, the spring coefficient k, and the axial force F during the first oscillation cycle all become constant m_0, b_0, k_0, and F_0, respectively. Therefore, Equation 1 is simplified into a constant coefficient ordinary differential equation

$$m_0\ddot{x} + b_0\dot{x} + k_0 x = F_0 \qquad (12)$$

This constant coefficient equation has an analytical solution as follows:

$$x = \frac{F_0}{k_0} + Ae^{-\varepsilon_0 t}\sin(\omega_0 t + \psi)$$

where

$$\varepsilon_0 = \frac{b_0}{2m_0} \quad \omega_0 = \sqrt{\frac{k_0}{m_0} - \varepsilon_0^2} \qquad (13)$$

and A along with ψ are coefficients determined by the initial droplet displacement and velocity depending on the exciting parameters. Based on Equation 13, the damping coefficient and spring constant can be calculated since the droplet mass, oscillation period, and amplitude all can be measured from the experiments. By adjusting the initial droplet mass m_0, the correlation between b/k and m can be determined.

To perform the calibration, experiments 1–4 are conducted by using Wave1. The experimental system and conditions are the same with that described in the first part of this investigation: 0.8-mm ER70S-6 welding wire, 15 L/min pure argon shielding gas, 6-mm wire extension, and bead-on-plate welding of mild steel (Ref. 1). The initial droplet mass/size is controlled by adjusting the growing duration T_g. The experimental parameters are listed in Table 1. The remaining parameters are fixed at I_g = 80 A, I_b = 30 A, T_{p1} = 3 ms, I_e = 120 Å, T_e = 3 ms, T_b = 30 ms, I_{fd} = 175 A, T_{fd} = 5 ms.

Damping Coefficient

According to Equation 13, the damping coefficient can be calculated as follows:

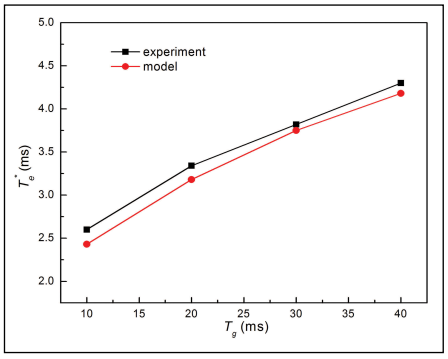

Fig. 14 — T^*_e under different T_g.

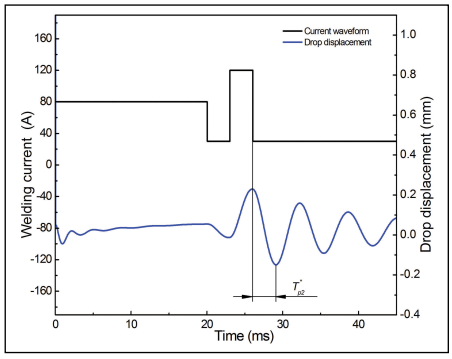

Fig. 15 — Example for predicting T^*_{p2}.

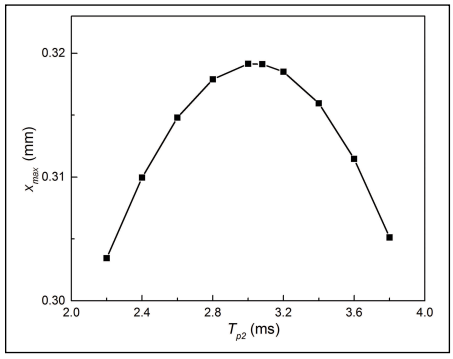

Fig. 16 — Effect of T_{p2} on the droplet oscillation/detachment.

$$b_0 = \frac{2m_0}{T_1} ln \frac{A_1}{A_2} \quad (14)$$

where T_1 is the oscillation period of the first oscillation cycle after the exciting pulse.

As shown in Fig. 6, A_1 and A_2 are the oscillation amplitude of the first and second oscillation cycle, respectively. The droplet oscillation period T_1 and the initial droplet mass m_0 are measured from the recorded high-speed image sequences. Using Equation 14, the damping coefficient in experiments 1–4 are calculated. The results are shown in Fig. 7. It can be seen that the damping coefficient is approximately at the same level when the droplet mass is increasing. Thereby, the damping coefficient is fixed at 0.0012 Ns/m in this study, which is the average of the measured values from experiments 1–4.

Spring Constant

Based on Equation 13, the droplet oscillation period of the first oscillation cycle T_1 is given by

$$T_1 = \frac{2\pi}{\omega_0} = \frac{4\pi m_0}{\sqrt{4k_0 m_0 - b_0^2}} \quad (15)$$

since the damping coefficient is only at 10^{-3} N·s/m, Equation 15 can be simplified to

$$T_1 = 2\pi\sqrt{m_0 / k_0} \quad (16)$$

the initial droplet mass m_0 and the droplet oscillation period of the first cycle T_1 are measured from experiments 1–4 and then the corresponding spring constant can be calculated, as shown in Fig. 8.

It can be seen that the droplet spring constant is approximately linearly increasing with the droplet mass such that the spring constant calculation model can be established by linearly fitting the experimental values using the Least Square method as follows:

$$k = 7.74 + 127961.29 \cdot m \quad (17)$$

Modeling Results and Discussion

A simulation program based on the model is developed in *Matlab/Simulink* to compute the dynamic droplet oscillation and detachment. The program structure is shown in Fig. 9. It can be seen that the dynamic droplet mass, radius, displacement, the spring constant, and the total detaching force can all be obtained from this numerical model. Forth-order Runge-Kutta algorithm is used to solve Equation 1. The physical constants used are listed in Table 2 (Refs. 13, 17, 18).

Optimal Exciting Phase Delay

In order to fully utilize the preoscillation before the exciting pulse, the optimal exciting phase delay under given growing parameters needs to be predicted first. According to the experimental study in the first part of this investigation, the optimal phase delay corresponds to the reversing moment of the droplet oscillation (Ref. 1). Given the current waveform parameters, the dynamic droplet displacement and forces can be calculated based on the above equations. By reading the time coordinate of the pre-oscillation reversing moment and the exciting end moment from the waveform and droplet displacement curves in Matlab, the optimal exciting phase delay T^*_{p1} at given waveform parameters can be determined. In order to guarantee the demonstration of the reversing moment, relatively large T_{p1} needs to be used. The calculation of the optimal exciting peak duration and optimal detaching phase delay will proceed in similar ways to guarantee

Table 1 — Growing Duration in Experiments 1–4

No.	T_g (ms)
1	10
2	20
3	30
4	40

Table 2 — Physical Constant Used in the Model

Symbol	Value	Unit	Description
C_1	2.885e–10	$m^3/(A\ s)$	Melting constant
C_2	5.22e–10	$m^3/(A\ \Omega s)$	Melting constant
r_w	0.0004	m	Wire radius
l_e	0.006	m	Wire extension
ρ_r	0.7836	Ω/m	Resistivity of Wire
ρ'	6800	kg/m^3	Density of liquid drop
ρ	7860	kg/m^3	Density of solid wire
μ_0	1.25664e–6	$kg\ m/A^2s^2$	Permeability of free space
γ	1.2	N/m	Surface tension coefficient

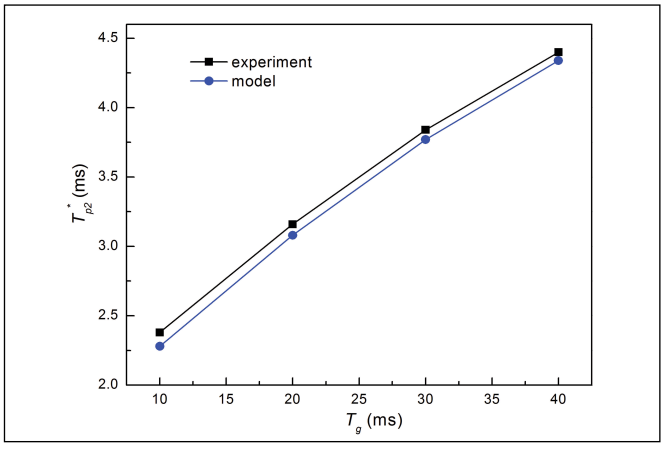

Fig. 17 — Comparison between modeling and experimental result on T^*_{p2}.

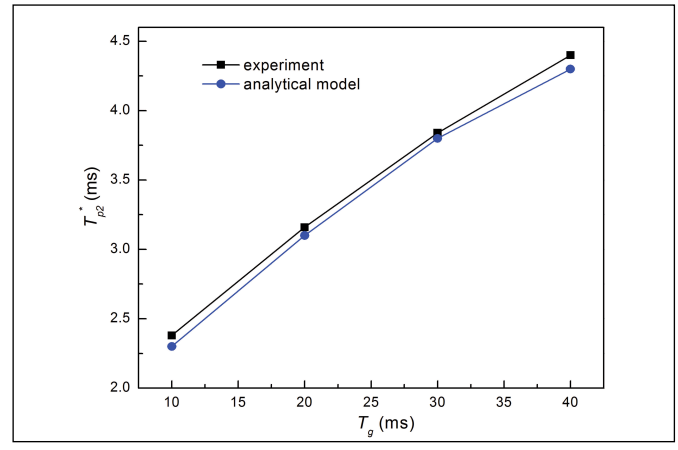

Fig. 18 — Prediction of T^*_{p2} *using the analytical model.*

the demonstration of the exciting peak moment and reversing moment of the main excited oscillation.

A simulation using Wave2 as the input to the model is first performed as a preliminary verification on the model with the following current waveform parameters: I_g = 80 A, T_g = 20 ms, I_b = 30 A, T_{p1} = 5 ms, I_e = 120 A, T_e = 3 ms, T_{p2} = 3 ms, I_d = 140 A, T_d = 5 ms, T_b = 20 ms, I_{fd} = 175 A, and T_{fd} = 5 ms. The time step for computation is 0.001 ms. The time cost for the computation on a common Desktop PC is only a few seconds. Figure 10A shows the droplet oscillation and detachment under the given current waveform parameters. The corresponding dynamic detaching force, droplet gravitational force, inertia force, electromagnetic force, and the droplet radius are shown in Fig. 10B–F, respectively. The calculated dynamic forces all correspond to the current waveform shown in Fig. 10A. One can see from Fig. 10C that the droplet gravitational force increases linearly in each substage, and a larger increasing rate associates with higher current. Since the wire diameter and the half angle are fixed, the electromagnetic force is determined by the current and droplet. It can be seen from Fig. 10D that the electromagnetic force is primarily determined by the welding current. Higher current produces larger electromagnetic force. While even the current is constant in each substage, the electromagnetic force still grows gradually, because the droplet radius is increasing. Figure 10E shows the dynamic inertia force. The step changes in Fig. 10E correspond to the rising or falling edges of the pulses in the current waveform which make sudden changes on the electromagnetic force and thus sudden changes on the droplet acceleration. The inertia force doesn't show direct correlation to the welding current. It is determined by the droplet displacement and velocity. Because the detaching pulse is applied when the droplet starts to move away from the wire tip, the droplet changes from being compressed to being elongated in the detaching peak time, and the direction of the inertia force is thus also changed. It can be seen that the excited droplet oscillation produces considerable inertia force, which is synchronized with the electromagnetic force produced by the detaching pulse and the total detaching force is thus significantly increased, as shown in Fig. 10B. Hence, the droplet is successfully detached under only 140 A detaching current. The detached droplet radius approximately equals that measured in the experiment using the same waveform parameters.

From Fig. 10A, one can see that the droplet is excited into a slight pre-oscillation under 80 A growing current. T_{p1} is intentionally set at 5 ms to demonstrate the reversing moment of the preoscillation, marked in Fig. 10A. By reading the time of the exciting end moment and the preoscillation reversing moment from the computed curves in *Matlab*, the corresponding T^*_{p1} can be obtained. In the case as Fig. 10A shows, T^*_{p1} is determined to be 2.8 ms. Using the same method, T^*_{p1} under different droplet mass (controlled by the growing duration) can be obtained. The modeling and corresponding experimental results are shown in Fig. 11. It can be seen that the droplet growing time changes in 10–40 ms; thus, the droplet diameter is within 1–1.6 mm, wide enough for discussing drop spray transfer characterized by relatively small droplet size. It can be calculated that the absolute modeling error on T^*_{p1} is only 0.07 ms, which indicates satisfactory modeling accuracy. When the initial droplet mass changes significantly in the wide range, T^*_{p1} does not change significantly, but are all within 2–4 ms. If the initial droplet size is controlled no larger than 1.25 mm corresponding to 80 A/20 ms growing pulse, T_{p1} can be roughly fixed at 2 or 3 ms as a quick set, while the utilization of the preoscillation is almost not compromised.

Optimal Exciting Peak Duration

Also using Wave2 as the input of the model, the exciting peak duration is first set at 30 ms, which is long enough to demonstrate the droplet dynamic response to the exciting pulse and gives a better understanding of its effect on the excited droplet oscillation. The model calculation result is shown in Fig. 12.

It can be seen that the droplet is first excited into a peak elongation and then goes into a forced oscillation during the long exciting peak period. As a contrast, the droplet oscillation during the base period after the exciting pulse can be considered as a free oscillation since the electromagnetic force under the base current is negligible. Figure 12 clearly demonstrates

that the droplet displacement and velocity at the end moment of the exciting pulse is exactly the initial condition of the consequent free oscillation. Since the forced oscillation during the exciting peak duration is damping, the maximum amplitude of the free oscillation after the exciting pulse can only be achieved if the exciting pulse ends at the elongation peak moment, i.e., the optimal exciting peak duration T^*_e corresponds to the elongation peak moment. Figure 13 demonstrates the effect of the exciting peak duration on the magnitude of the free oscillation. The growing current is fixed at 80 A with 20 ms duration. The exciting peak current is fixed at 120 A, while the exciting peak duration changes from 2–5 ms. It can be seen that the droplet oscillation magnitudes under 3 and 4 ms exciting peak durations are approximately even at the maximum level. The droplet oscillation under 2 ms exciting peak duration is a little weaker, while that under 5 ms exciting peak duration is significantly weaker. These results agree with those of the experimental examination in Ref. 8.

Through the model based on Equation 1, T^*_e can be obtained by intentionally setting relatively long exciting peak duration. Figure 14 shows a comparison between the experiment-tested and model-predicted results under different droplet masses (controlled by the growing duration). The figure demonstrates that the experimental results are all slightly larger than the corresponding model-predicted ones. The maximum absolute error is up to 0.17 ms. This is caused by the limited rising speed of the real welding current when it is changed from the base to peak. In general, the rising time is approximately 1 ms such that the oscillation peak time becomes a little longer than that calculated from the model. However, such a level of difference on the exciting peak duration will not significantly affect the amplitude of the free oscillation after the exciting pulse. Here, the exciting peak duration can also be fixed at 3 ms as a quick set, as long as the growing parameters are properly selected to control the droplet size not exceeding 1.25 mm.

Optimal Detaching Phase Delay

The detaching phase delay is the most important parameter because it determines the synchronization between the detaching pulse and droplet downward momentum. The first part of this investigation (Ref. 1) has confirmed that the feature detaching phase delay corresponds to the reversing moment of the excited free droplet oscillation is the optimal detaching phase delay. This conclusion is verified here based on the model using I_g = 80 A, T_g = 20 ms, I_b = 30 A, T_{p1} = 3 ms, I_e = 120 A, and T_e = 3 ms. Figure 15 shows the model-predicted T^*_{p2} is 3.08 ms. Using Wave2 as the input of the model, a group of T_{p2} around this feature value are used to perform simulations to verify the optimality of the feature detaching phase delay. Here I_d is set at 110 A. Thus, it will elongate the droplet, but the elongation is not strong enough to detach the droplet. Hence, the peak droplet displacement during the detaching pulse under different T_{p2} denoted as x_p can be collected to evaluate the effect of T_{p2}. The results are shown in Fig. 16. It can be seen that the maximum x_p is achieved when T_{p2} equals the predicted T^*_{p2}, 3.08 ms. Overall, the simulation results support that the feature phase delay corresponding to the oscillation reversing moment is the optimal for maximum enhancement on the droplet detachment.

Figure 17 shows a comparison between the modeling and the experimental results of T^*_{p2} under different initial droplet masses controlled the growing duration. It can be calculated that the maximum error is only 0.1 ms, and the average error calculated from the four samples is only 0.058 ms. Such a low level of prediction error indicates satisfactory accuracy of the model. Here, T^*_{p2} under different growing parameters cannot be simply fixed at a certain value as a quick set, because the utilization of the droplet downward momentum is sensitive to the selection of T_{p2}. The tolerance range of T_{p2} for maximum utilization of the downward momentum was experimentally estimated to be [T^*_{p2} – 0.2, T^*_{p2} + 0.4] ms in the first part of this investigation (Ref. 1).

Analytical Model on Droplet Oscillation

Model Derivation

From the above results and analysis, one can see that the established model gives a comprehensive understanding on the dynamic droplet oscillation and detachment in the enhanced active metal transfer control. The dynamic droplet size/mass, droplet motion, and the forces exerted on the droplet can be computed, and the computation time is only several seconds. However, if possible, a simpler analytical model with acceptable accuracy would be more appreciated. Since the numerical modeling results imply that T^*_{p1} and T^*_e can both be quickly set as long as the initial droplet size is controlled within 1–1.3 mm, the analytical model will only aim at the prediction of T^*_{p2},which determines the optimal synchronization of the detaching pulse and the droplet downward momentum. To this end, the following approximations are applied to simplify the original model and thus to avoid numerical computations as follows:

1. Set the damping coefficient b to zero. Since the viscous damping in droplet oscillation was found to have a negligible effect on calculating the droplet oscillation frequency compared with other factors such as surface tension and gravity (Ref. 9), the damping coefficient can be set to zero in predicting T^*_{p2}.

2. Use a constant droplet mass to replace the time-varying droplet mass during a short period. As the same assumption used for the coefficient calibration, the droplet mass during the exciting peak period and the first free oscillation cycle is considered to be constant and equals the value measured at the end of exciting pulse, denoted as m_0. Based on Equations 3 and 4, m_0 can be calculated by

$$m_0 = \rho \begin{bmatrix} \left(C_1 I_g + C_2 \rho_r l_e I_g^2\right) T_g \\ + \left(C_1 I_{b1} + C_2 \rho_r l_e I_{b1}^2\right) T_{b1} \\ + \left(C_1 I_e + C_2 \rho_r l_e I_e^2\right) T_e \\ + \left(C_1 I_d + C_2 \rho_r l_e I_d^2\right) T_{re} \end{bmatrix} \quad (18)$$

where T_{re} represents the residual peak duration of the forced detaching pulse. For 5 ms forced detaching peak duration, T_{re} equals 0.5 ms approximately.

Finally, the model depicting the droplet's dynamic response to the exciting pulse can be expressed as:

$$m_0\ddot{x}+k_0x=F(t) \tag{19}$$

$$F(t)=\begin{cases} F_{em}(I_e)-F_{em}(I_b) & 0\le t\le T_e \\ 0 & t\ge T_e \end{cases}$$

Define $w_0\sqrt{k_0/m_0}$, *thus the analytical solution of Equation 19 is derived to be*

(20)

$$x(t)=\begin{cases} \dfrac{F_{em}(I_e)-F_{em}(I_b)}{k_0}\left[1-\cos\omega_0 t\right], & 0<t\le T_e \\ \dfrac{F_{em}(I_e)-F_{em}(I_b)}{k_0}\left[\cos\omega_0(t-T_e)-\cos\omega_0 t\right], & t\ge T_e \end{cases}$$

(21)

From Equation 21, T^*_{p2} under given growing and exciting parameters is derived to be

$$T^*_{p2}=\frac{3}{4}T_1-\frac{1}{2}T_e,\qquad T_1=2\pi\sqrt{m_0/k_0} \tag{22}$$

The comparison between the analytical modeling and experimental results is shown in Fig. 18. It can be seen that the analytical model also shows satisfactory accuracy in predicting T^*_{p2} since the maximum absolute error is only 0.1 ms.

Conclusions

1. A theoretical model on the dynamic droplet oscillation and detachment in the enhanced active metal transfer control is established based on the mass-spring system. The critical coefficients, i.e., the spring constant and damping coefficient, are experimentally calibrated. It is found that the damping coefficient is approximately independent of the droplet mass, but the spring constant increases with the droplet mass linearly.

2. The model is numerically computed. The effects of the critical waveform parameters on the droplet oscillation/detachment are analyzed based on the model. The optimal exciting /detaching phase delay corresponds to the reversing moment of the droplet oscillation. The optimal exciting peak duration corresponds to the elongation peak moment. These results agree with those from the experimental study in the first part of this paper.

3. The numerical model enables one to predict the critical waveform parameters at adequate speed and accuracy, and can be used to effectively determine the waveform parameters for the enhanced active metal transfer control. The exciting phase delay and exciting peak duration can both be fixed as quick set as long as the growing parameters are properly selected such that the droplet size be relatively small as desired with the needed drop spray transfer.

4. An analytical model on the excited droplet oscillation has also been established through acceptable approximations such that the most important parameter, i.e., the optimal detaching phase delay, can be analytically calculated with adequate accuracy.

Acknowledgments

This work is financially supported by the State Key Laboratory of Advanced Welding and Joining, Harbin Institute of Technology, Harbin, China and the National Science Foundation under grant CMMI-0825956. J. Xiao greatly appreciates the scholarship from China Scholarship Council (CSC) that funded his visit to the University of Kentucky to conduct this research.

References

1. Xiao, J., Zhang, G. J., Zhang, W. J., and Zhang, Y. M. 2014. Active metal transfer control by utilizing enhanced droplet oscillation Part 1: Experimental study. *Welding Journal* 93(8): 282-s to 291-s.

2. Thomsen, J. S. 2006. Control of pulsed gas metal arc welding. *International Journal of Modelling, Identification, and Control* 1(2): 115–125.

3. Kim, Y. S., and Eagar, T. W. 1993. Metal transfer in pulsed current gas metal arc welding. *Welding Journal* 72(7): 279-s to 287-s.

4. Amin, M. 1983. Pulse current parameters for arc stability and controlled metal transfer in arc welding. *Metal Construction* 15: 272–278.

5. Jacobsen, N. 1992. Monopulse investigation of droplet detachment in pulsed gas metal arc welding. *Journal of Physics D: Applied Physics* 25: 783–797.

6. Zhang, Y. M., Liguo, E., and Kovacevic, R. 1998. Active metal transfer control by monitoring excited droplet oscillation. *Welding Journal* 77(9): 388-s to 395-s.

7. Zhang, Y. M., and Liguo, E. 1999. Method and system for gas metal arc welding. U.S. Patent #6,008,470.

8. Xiao, J., Zhang, G. J., Zhang, Y. M., et al. 2013. Active droplet oscillation excited by optimized waveform. *Welding Journal* 92(7): 205s to 217-s.

9. Choi, J. H., Lee, J., and Yoo, C. D. 2001. Dynamic force balance model for metal transfer analysis in arc welding. *Journal of Physics D: Applied Physics* 34: 2658–2664.

10. Jones, L. A., Eagar, T. W., and Lang, J. H. 1998. A dynamic model of drops detaching from a gas metal arc welding electrode. *Journal of Physics D: Applied Physics* 31: 107–123.

11. Wu, C. S., Chen, M. A., and Li, S. K. 2004. Analysis of excited droplet oscillation and detachment in active control of metal transfer. *Computational Materials Science* 31(1-2): 147–154.

12. Chen, M. A., Wu, C. S., Li, S. K., and Zhang, Y. M. 2007. Analysis of active control of metal transfer in modified pulsed GMAW. *Science and Technology of Welding and Joining* 12(1): 0–14.

13. Lesnewich, A. 1958. Control of melting rate and metal transfer in gas shielded metal arc welding, Part 1: Control of electrode melting rate. *Welding Journal* 37(9): 343-s to 353-s.

14. Amson, J. C. 1965. Lorentz force in the molten tip of an arc electrode. *British Journal of Applied Physics*, 16: 1169–1179.

15. Kim , Y. S., and Eagar, T. W., 1993. Analysis of metal transfer in gas metal arc welding. *Welding Journal* 72(6): 269-s to 277-s.

16. Huang, Y., Shao, Y., and Zhang, Y. M. 2012. Nonlinear modeling of dynamic metal transfer in laser-enhanced GMAW. *Welding Journal* 91(5): 140-s to 148-s.

17. Choi, S., Kim, Y. S., and Yoo, C. D. 1999. Dimensional analysis of metal transfer in GMA welding. *Journal of Physics D: Applied Physics* 32: 326–334.

18. Naidu, D. S., Moore, K. L., Yender, R., and Tyler, J. 1997. Gas metal arc welding control: Part 1 — Modeling and analysis. *Nonlinear Analysis, Methods and Applications* 30(5): 3101– 3111.